Cyclic performance of Fe-based shape memory alloy buckling-restrained brace sub-assemblages

Ahmad Fayeq Ghowsi[1], Dipti Ranjan Sahoo[2], P. C. Ashwin Kumar[3]

[1] Ph.D. Student, Department of Civil Engineering, Indian Institute of Technology Delhi, New Delhi-110016, India.
[2] Associate Professor, Department of Civil Engineering, Indian Institute of Technology Delhi, New Delhi-110016, India.
[3] Assistant Professor, Department of Earthquake Engineering, Indian Institute of Technology Roorkee, Roorkee-247667, India.

ABSTRACT

Buckling-restrained braces (BRBs) exhibit high axial load-resisting capacity, nearly symmetric hysteretic response, and better displacement ductility under cyclic loading. However, due to the slender core elements of BRBs, excessive post-earthquake residual drift response is expected in buckling-restrained braced frames (BRBFs) as compared to other lateral force-resisting systems. This study is focused on the evaluation of cyclic performance of BRBs made of ferrous (Fe)-based shape-memory alloy (SMA). The super-elasticity characteristic of SMA plates is used to enhance the self-centering potential of BRBs. To minimize the cost of SMA plates, reduced-length BRBs are connected in series with the hot-rolled steel tubular members along their lengths. These tubular members are designed to remain elastic prior to the fracture of BRB core plates. An experimental investigation is carried out to investigate the cyclic performance of six brace sub-assemblages in accordance with AISC 341-10 loading protocol. The BRB core lengths as well as the detailing of core plates are varied in the test specimens. These braces are designed as all-steel BRBs in which hot-rolled angle sections with bolted connections are adopted as the restraining elements. The main parameters studied are the hysteretic response, displacement ductility, and the cumulative displacement ductility of braces. Hysteretic response of test specimens showed the self-centering capability of BRBs. The energy dissipation potential and mode of failure of test specimens are also discussed. Test results showed that the use of welding connections between the core and elastic segments significantly reduced the displacement ductility of these Fe-based SMA BRBs.

Keywords: Buckling-restrained braces; Displacement ductility; Energy dissipation; Self-centering braces; Shape memory alloy.

INTRODUCTION

Steel concentrically braced frames (CBFs) are usually used to enhance the lateral resistance and stiffness a structure under earthquake and wind loadings. However, the compression buckling of conventional steel braces results in the limited ductility, the reduced energy dissipation, and unsymmetrical hysteretic response. Buckling-restrained braces (BRBs) eliminate the buckling instability prior to the compression yielding under axial loading [1]. Thus, the core elements of BRBs exhibit significant inelastic strain under tension as well as compression loading and undergo the higher mode buckling. Hollow steel sections filled with cement mortar are typically used as the restraining elements to the central core elements of the conventional BRBs [2]. Recently, all-steel BRBs are becoming popular in which the restraining systems are prepared using steel elements [3]. Relatively, all-steel BRBs can be made lighter in weight as compared to the conventional BRBs [4]. Extensive studies have been conducted to investigate the effect of stopper on the BRB yielding core element's ductility [5], the effectiveness of bolted restraints [6], the influence of unbonding material between the yielding core element and restraining element [3] on the cyclic performance of all-steel BRBs. Numerical and analytical studies on the effect of loading protocol and parameters of restraining element [7], the influence of friction, gap width, core slenderness ratio, and the position and detailing of stoppers, and the estimation of design forces on the bolted connections of the restraining element [8] have also been conducted. Fish-bone shaped all-steel BRBs have shown to perform better under cyclic loading as compared to the conventional BRBs [9].

Past studies [10,11] have shown that the lack of re-centering capability of BRBs may result in the excessive post-earthquake residual displacement of the braced frame. This may not be cost-effective in terms of repair and retrofit [12]. In order to minimize this effect, some modifications may be carried out in the development of BRBs so as to develop self-centering BRB (SC-BRB) systems which can provide the re-centering capability to the buckling-restrained braced frames (BRBFs) [13]. The application of post-tensioning (PT) rods for to enhance the self-centering capability of the structural system has been investigated [14].

A self-centring energy dissipation system using friction devices and dual tube self-centering with aramid PT has been developed recently [15]. Three specimens of lightweight dual-tube SC-BRB using basalt fibre-reinforced polymer as pretention tendon material under quasi-static loading has also been tested previously [16], [17]. Test result showed the flag-shaped hysteretic response of braces exhibiting the better self-centering capability. Finite element analysis on dual tube SC-BRB using polymer pretension [18], design parameters of SC-BRB using a rheological model [19] are some of the work directed towards improving the self-centering capability of BRBFs. This present paper deals with the experimental study of light weight all-steel BRB with self-centering capability provided using Fe-based shape-memory alloy.

SCOPE AND OBJECTIVES

In this paper, an experimental study has been conducted on all-steel BRB with a short-core Fe-based shape memory alloy (FSBRB). FSBRB is made of steel with four angle sections as restrainers to confine the core from the global as well torsional buckling. An elastic segment is used along the length of the brace to minimize the length of BRB core elements. The core segment of BRB uses Fe-based shape memory alloy (SMA) for the purpose of re-centering capability of BRB. In this study, cyclic tests of five FSBRB specimens and one coupon FSBRB sample has been conducted to validate this new concept and investigate the hysteretic behaviour with self-centring capability. The sub-assemblages of FSBRB specimens are subjected to quasi-static displacement-controlled loading in accordance with AISC 341 [20] provisions.

DESIGN AND CONCEPT OF (FSBRB)

Five FSBRB specimens of 3534 mm long have been considered in this study for the sub-assemblage tests. Figure 1(a) shows the dimensions of different components of FSBRB specimen. The thickness of the core plate and the end elastic cruciform plate is 9 mm. The length of core segment is varied in each specimen along with the elastic brace segment to maintain the same total length of assembly for all specimens. The SMA is used only in the yielding length of the core to increase the cost effectiveness. The ends of the core segment is inserted inside the transition and elastic zones of BRB to achieve the required strength. The penetrated ends of the core into the elastic end transitions zones with cruciform shape is as shown in Figure 1(b). The welding lengths are varied in the test specimens based on the ultimate strengths of the core segments. For restraining the core segment from the global and torsional buckling, four angles are bolted back to back with gap controlling plates between every two angles as shown in Figure 1(b). The desired gap is maintained between the core and the restrainer plates in order to allow the core plates to undergo the higher buckling modes corresponding to the high compressive axial load. A stopper has been provided in the brace for preventing the relative movement of the restraining element with respect to the core segment. Polytetrafluoroethylene (PTFE) sheets of 1 mm thick as the unbonding material are wrapped over the core element to minimize the friction between the core and the restraining element surfaces. Additionally, in some cases, the cruciform-shaped stiffeners have been extended over the weak axis of the core segment to prevent the end failure of the core. Table 1 summarizes the details of specimen considered in this study. Relatively longer end and transition segments have been adopted at one end of BRB as shown in Figure 1.

The test setup of the overall sub-assemblage FSBRB specimen subjected to cyclic loading is shown in Figure 2. The brace ends are fixed and not allowed to rotate. The bottom of column and the braced end is connected to a plate which is fastened to the rigid strong floor of the laboratory. A servo-controlled hydraulic actuator of 500 kN capacity is used to apply the cyclic loading to the FSBRB specimens.

Table 1. Details of test specimens.

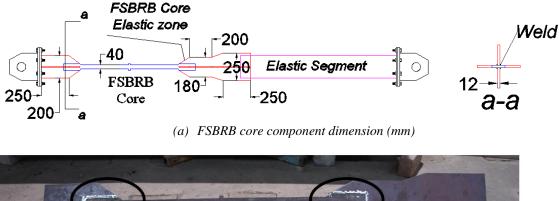| Specimen	Core Length (mm)	Gap of the core and restrainers (mm)	Position of stoppers	Stiffeners over the core welding
FSBRB1	880	1	Centre	NA
FSBRB2	730	3	Centre	Left ends
FSBRB3	580	3	Centre	Both ends
FSBRB4	620	3	End	Both ends
FSBRB5	480	3	End	Both ends

MATERIAL PROPERTY

Initially, monotonic tests are carried out on three coupon specimens of FSBRB as shown in Figure 3. The yield stress for all three coupons is noted as 680 MPa, whereas the ultimate stress values are noted in the range of 1000 to 1200 MPa. The average value of Young's Modulus is estimated as 200GPa. The maximum ultimate strain is obtained in the range of 48-58%. A sudden fracture without any degradation is noted during the tension tests of all three coupons. Additionally, a component level coupon test of FSBRB named here as CFSBRB has been conducted under cyclic loading. The test setup of the specimen is as shown in Figure 4(a). The dimension of the test specimen in millimeter is as shown in Figure 4(b). The CFSBRB specimen is subjected

to cyclic loading similar to that used for testing of BRBs [20]. The loading protocol applied is as shown in Figure 5(a). The SMA rod has been shaped to represent a small BRB specimen with a transition zone at the ends of the core middle segment and a stopper at the centre. A steel restrainer has been provided around the SMA core and a constant gap has been provided between the core and restraining element. The hysteretic response of CFSBRB is shown in Figure 5(b). Test results showed the nearly-symmetrical hysteresis response with the higher ductility and the re-centering ability. After completion of two cycles of 8% axial strain, the specimen is fractured near to the stopper position. Figure 5(c) shows the fractured SMA core.

(a) FSBRB core component dimension (mm)

(b) FSBRB penetrated welded core and gap control plates
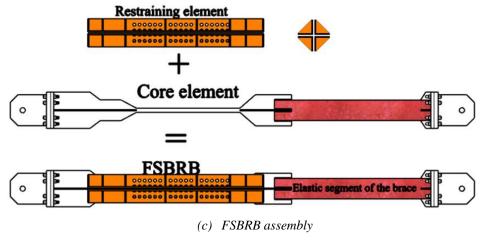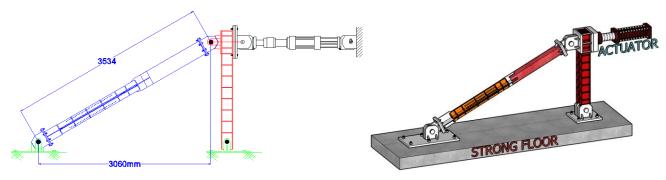

(c) FSBRB assembly

Figure 1. Components of FSBRB.
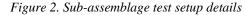
EXPERIMENTAL SETUP

Figure 6(a) shows the test setup used for large-scale FSBRB specimen. The brace ends connections are fixed and restrained against the rotation. A 500 kN capacity actuator is used to apply the loading in displacement-control mode. The angle of inclination of braces is kept at 30 degrees relative to the ground for all setups. The axial displacement of the brace is measured

by the actuator as well as string potentiometer (SP) fixed along the brace length. A string potentiometer has also been used in the transverse direction at point of connection of elastic brace and BRB to measure the lateral displacement, which can occur in case of global buckling and out of plane buckling. As shown in Figure 6(b), the selected loading protocol consists of four cycles for each story drift of 0.05, 0.15, 0.3, and 0.5% and two cycles for each deformation of 1.0, 1.5, and 2.0% drift levels. The strain rate has been fixed at 0.25mm/sec for the first 12 cycles and it has been increased to 0.5mm/sec for the rest of the cycles, until fracture.

| *(a) FSBRB sub-assemblage dimension* | *(b) FSBRB sub-assemblage full setup* |

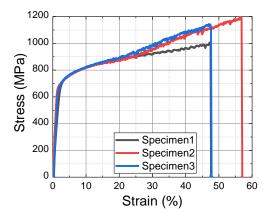*Figure 2. Sub-assemblage test setup details*

Figure 3. Tensile stress-strain characteristics of three FSBRB core coupons.
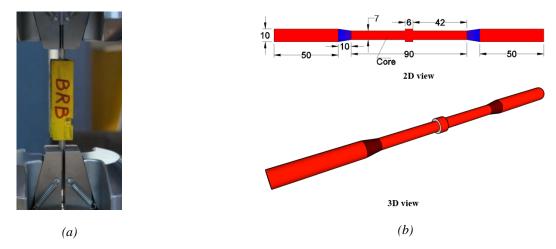

| *(a)* | *(b)* |

Figure 4. BRB coupons under cyclic loading (a) Specimen setup (b) 2D and 3D view of the coupon specimen of FSBRB (dimensions in mm)

TEST RESULTS AND DISCUSSION

Table 2 summarizes the axial stress-core strain (hysteretic) response, failure mode, and the location of fracture noted in the five sub-assemblage specimens of FSBRBs. The self-centering capability of these specimens is noted similar to that of the CFSBRB specimen. All the specimens exhibited stable hysteretic behavior without degradation with a positive incremental stiffness. As expected, the brace strength in compression has been obtained greater than tension strength due to friction, higher mode, and Poisson's ratio effect [7]. Sharp drop in compression strength is noted due to shift from static to kinematic friction. No global and local buckling is noted in the end plates as well as the elastic segments of braces. Additionally, failure of bolts and connections has not occurred. In all the cases, the fracture occurred within the SMA core segment near the welding regions.
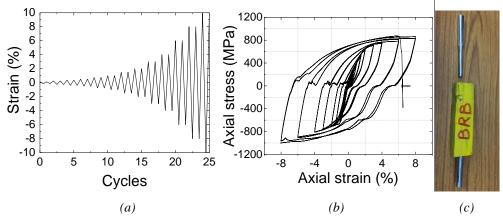

Figure 5. (a) Loading protocol (b) Hysteretic response of CFSBRB.

For specimen FSBRB1, the fracture occurred near the transition zone at 2.6% of axial strain, which corresponds to 1.5% of story drift. The higher-mode buckling of the core plate is not visible at this stage. FSBRB2 specimen is the repaired version of FSBRB1 with crossed stiffeners extended up to 150 mm over the core on the weak surface and with increased gap between the core and restraining element from 1 to 3 mm on each side. The results showed gains of additional 2% axial strain, which corresponds to 2.1% story drift. The fracture for this specimen occurred near the transition zone and welding spots on the opposite ends of the repaired segment. A lower compression capacity relative to the tension hysteretic response has been observed due to the residual strain at the fracture point from the FSBRB1 test. The previous elongation has been considered as the zero-reference point for FSBRB2 and the current displacement has been added to the previous strain in the tension direction. FSBRB3 is the repaired version of FSBRB2 by welding the crossed stiffener similar to the repair of FSBRB2 in the opposite direction. The results showed additional 2.64% axial strain and 1% of story drift. The fracture occurred at the center of the core element next to the extruded stoppers. FSBRB4 specimen consists of a new core with extended crossed stiffener over the weak surface of the core up to 50 mm, without extruded stopper. The stoppers are considered out of the core as contact at bottom of the brace prevents the restrainers from sliding on the inclined direction toward the bottom end. Relatively better result has been obtained in this case with 3.7% of axial strain corresponding to 1.5% of story drift due the short length of the core segment. As expected from the previous cases, the fracture occurred at the bottom end of the cored near the welding spots without significant higher mode buckling in the core element. FSBRB5 with a new core similar to FSBRB4 had a different length of yielding core with restrained elastic ends zones. The result obtained for this specimen has the highest ductility with 4.78% axial strain reaching the target cumulative ductility [20].
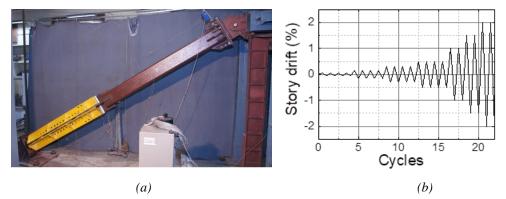

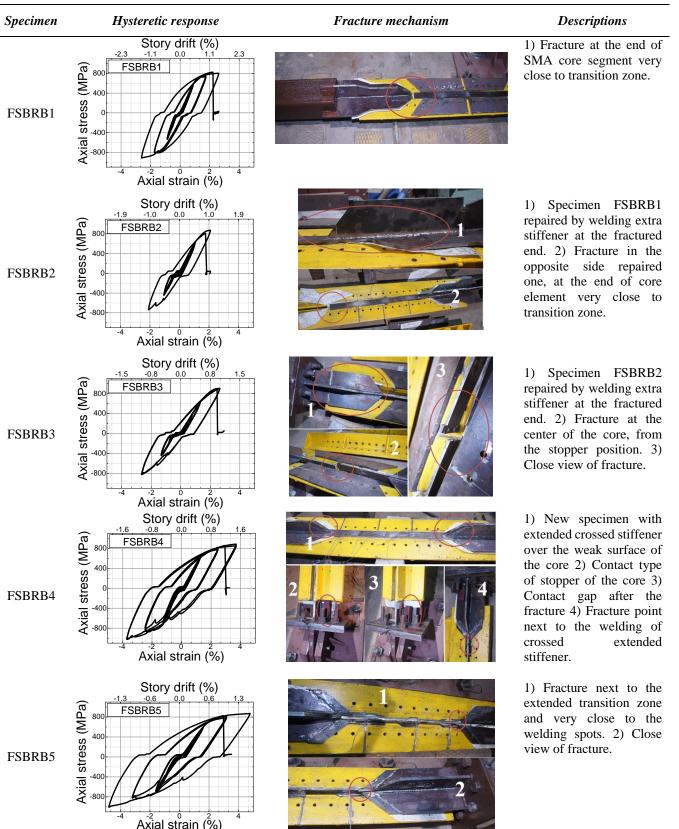*Figure 6. (a) FSBRB sub-assemblage test setup (b) Loading protocol*

5

Table 2. Summary of hysteretic response and fracture mechanism of FSBRBs.

Specimen	Hysteretic response	Fracture mechanism	Descriptions
FSBRB1			1) Fracture at the end of SMA core segment very close to transition zone.
FSBRB2			1) Specimen FSBRB1 repaired by welding extra stiffener at the fractured end. 2) Fracture in the opposite side repaired one, at the end of core element very close to transition zone.
FSBRB3			1) Specimen FSBRB2 repaired by welding extra stiffener at the fractured end. 2) Fracture at the center of the core, from the stopper position. 3) Close view of fracture.
FSBRB4			1) New specimen with extended crossed stiffener over the weak surface of the core 2) Contact type of stopper of the core 3) Contact gap after the fracture 4) Fracture point next to the welding of crossed extended stiffener.
FSBRB5			1) Fracture next to the extended transition zone and very close to the welding spots. 2) Close view of fracture.

Table 3 summarizes the strength-adjustment factors of BRB segments in test specimens. Based on each core length of L_c, (total length of work point to work point of the brace *L)* and material properties from the coupon tests results, the yield displacement

Δ_y of the core element has been calculated. The maximum tensile force of T_{max} and the maximum compressive force C_{max} in axial direction of the brace member have been computed during the test cyclic loading of hysteretic responses. The compressive adjustment factor, β has been calculated based on Eq. (1), as the ratio of maximum compressive force C_{max} to the maximum tensile force at peak forces of same cycles after the yield. Table 3 summarizes the compressive adjustment factor for each specimen, except FSBRB2 and FSBRB3, in which the β values is less than one as it has been the repaired version of FSBRB1.

$$\beta = \frac{C_{max}}{T_{max}} \tag{1}$$

More importantly, in all the cases the β value is less than 1.3 in same cycles of tensions and compression, which is the target value for BRB test specimens. Strain-hardening adjustment factor, ω is defined as the ratio of the maximum tensile force T_{max} on the axial direction to the yield strength of the core based on coupon tests result. Mathematically,

$$\omega = \frac{T_{max}}{F_{yc} A_{yc}} \tag{2}$$

Where, F_{yc} is the yield strength of the core element from the coupon tests, and A_{yc} is the cross-section area of the core element. The maximum displacement ductility of μ is calculated based on Eq. (3) which is the ratio of the absolute maximum deformation $\left| \Delta_{T_{max},C_{max}} \right|$ of the FSBRBs to the yield deformation Δ_{yc} of the core element. Table 3 summarizes the maximum ductility of all the specimens.

$$\mu = \frac{\left| \Delta_{T_{max},C_{max}} \right|}{\Delta_{yc}} \tag{3}$$

The displacement cumulative ductility is calculated based on Eq. (4) as it represents the combined inelastic deformation of the brace till fracture. Table 3 summarizes the cumulative displacement η_c for all the specimens.

$$\eta_c = \sum \left[\frac{2(\left| \Delta_{T_{max}} \right|_i + \left| \Delta_{C_{max}} \right|_i)}{\Delta_{yc}} - 4 \right] \tag{4}$$

The BRB cumulative deformation requirement for the axial deformation is to achieve 200 times the yield deformation [20]. In the literature [21], a cumulative ductility of 140 times the yield deformation for the sub-assemblage tests has been suggested. The FSBRB1, FSBRB2, and FSBRB3 and all other specimens achieved this requirement.

Table 3. Comparison of strength adjustment parameters of FSBRBs.

Specimen	Lc (mm)	Lc/L	Δy (mm)	Py (kN)	Tmax (kN)	Cmax (kN)	ω	β	βω	μc	ηc
FSBRB1	880	0.25	2.99	244.8	299	327	1.22	1.093	1.33	7.68	96
FSBRB2	730	0.21	2.48	244.8	309.5	264.8	1.26	--	--	6.04	69 293
FSBRB3	580	0.16	1.97	244.8	317.6	298	1.29	--	--	7.61	128
FSBRB4	620	0.18	2.11	244.8	310	366	1.27	1.18	1.50	10.66	195
FSBRB5	480	0.14	1.63	244.8	312	358	1.27	1.15	1.46	13.5	222
CFSBRB	84	0.4	0.29	26.17	33.6	38.5	1.28	1.15	1.47	23.17	483

CONCLUSIONS

Based on experimental and analytical studies, the following conclusions can be drawn:

- The proposed FSBRBs exhibited the re-centering capability in all test specimens.
- The FSBRB specimens exhibited a lesser compressive adjustment factor for all the cases and achieved the targeted cumulative ductility of 140.
- A new stopper arrangement has been proposed for the steel BRB, which shows better cumulative ductility and maximum strain in the core, relative to the conventional stoppers at the center the core element for all-steel BRBs.
- The Fe-SMA material without heat and welding spots is showing excellent ductility and energy dissipation capacity. However, the material degraded considerably while cutting and welding on the core.
- Using crossed stiffener over the core on weak surface increased the ductility capacity of the core element.

REFERENCES

[1]   Wu, A.-C., Lin., P.-C., and Tsai, K.-C. (2014). "High-mode buckling responses of buckling-restrained brace core plates." *Earthquake Engineering and Structural Dynamics*, 43(3), 375–393.

[2]   Kim, D., Lee, C., and Jin, S. (2015). "Prediction of hysteretic response of group-bolted connections subjected to cyclic eccentric shear loading." *8th Int. Symp. Steel Struct. Novemb. 5-7, 2015*, pp. 287–288, 2015.

[3]   Chen, Q., Wang, C. L., Meng, S., and Zeng, B. (2016). "Effect of the unbonding materials on the mechanic behavior of all-steel buckling-restrained braces." *Engineering Structures*, 111, 478–493.

[4]   Dusicka, P., and Tinker, J. (2013). "Global restraint in ultra-lightweight buckling-restrained braces." *Journal of Composites for Construction*, 17(1), 139–150.

[5]   Wang, C. L., Usami, T., Funayama, J., and Imase, F. (2013). "Low-cycle fatigue testing of extruded aluminium alloy buckling-restrained braces." *Engineering Structures*, 46, 294–301.

[6]   Metelli, G., Bregoli, G., and Genna, F. (2016). "Experimental study on the lateral thrust generated by core buckling in bolted-BRBs." *Journal of Constructional Steel Research*, 122, 409–420.

[7]   Ghowsi, A. F., and Sahoo, D. R. (2018). "Effect of loading history and restraining parameters on cyclic response of steel BRBs." *International Journal of Steel Structures*, No. 0123456789.

[8]   Dehghani, M., and Tremblay, R. (2017). "An analytical model for estimating restrainer design forces in bolted buckling-restrained braces." *Journal of Constructional Steel Research*, 138, 608–620.

[9]   Jia, L. J., Ge, H., Maruyama, R., and Shinohara, K. (2017). "Development of a novel high-performance all-steel fishbone shaped buckling-restrained brace." *Engineering Structures*, 138, 105–119.

[10]   Clark, P. W., Kasai, K., Aiken, I. D., and Kimura, I. (2000). "Evaluation of design methodologies for structures incorporating steel unbonded braces for energy dissipation." In *12th World Conference on Earthquake Engineering*, Auckland, New Zealand.

[11]   Ghowsi, A. F., and Sahoo, D. R. (2015). "Fragility assessment of buckling-restrained braced frames under near-field earthquakes." *Steel and Composite Structures*, 19(1), 173–190.

[12]   Dolce, M. and Cardone, D. (2006). "Theoretical and Experimental Studies for the Application of Shape Memory Alloys in Civil Engineering." *Journal of Engineering Materials and Technology*, 128(3), 302.

[13]   Eatherton, M. R., Fahnestock, L. A., and Miller, D. J. (2014). "Self-centering buckling restrained brace development and application for seismic response mitigation." In *NCEE 2014 - 10th U.S. Natl. Conf. Earthq. Eng. Front. Earthq. Eng.*, Anchorage, Alaska.

[14]   Christopoulos, C., Tremblay, R., Kim, H., and Lacerte, M. (2008). "Self-Centering Energy Dissipative Bracing System for the Seismic Resistance of Structures." 134(1), 96–107.

[15]   Erochko, J., Christopoulos, C., and Tremblay, R. (2015). "Design, testing, and detailed component modeling of a high-capacity self-centering energy-dissipative brace." *Journal of Structural Engineering*, 141(8).

[16]   Zhou, Z., He, X. T., Wu, J., Wang, C. L., and Meng, S. P. (2014). "Development of a novel self-centering buckling-restrained brace with BFRP composite tendons." *Steel and Composite Structures*, 16(5), 491–506.

[17]   Zhou, Z., Xie, Q., Lei, X. C., He, X. T., and Meng, S. P. (2015). "Experimental Investigation of the Hysteretic Performance of Dual-Tube Self-Centering Buckling-Restrained Braces with Composite Tendons," *Journal of Composites for construction*, 19(6).

[18]   Xie, Q., Zhou, Z., Huang, J. H., Zhu, D. P., and Meng, S. P. (2017). "Finite-Element Analysis of Dual-Tube Self-Centering Buckling-Restrained Braces with Composite Tendons." *Journal of Composites for construction*, 21(3).

[19]   Zhou, Z., Xie, Q., Meng, S. P., Wang, W. Y., and He, X. T. (2016). "Hysteretic Performance Analysis of Self-Centering Buckling Restrained Braces Using a Rheological Model." *Journal of Engineering Mechanics,* 142(6).

[20]   ANSI/AISC 341. (2010). Seismic provisions for structural steel buildings. Chicago, Illinois.

[21]   AISC/SEAOC. (2001). Recommended provisions for buckling-restrained braced frames. Chicago, Illinois.